



20 Running title: Factor analysis for wheat

21

22 Keywords: Bayesian network, confirmatory factor analysis, exploratory factor analysis,  
23 multi-trait, wheat

24

25 ORCID: 0000-0002-2562-2741 (MM), 0000-0002-4959-0481 (MB), 0000-0002-6861-0193 (WH),  
26 0000-0002-8923-9733 (HY), and 0000-0002-3567-6911 (GM).

27

## 28 Abstract

29 Inferring trait networks from a large volume of genetically correlated diverse phenotypes  
30 such as yield, architecture, and disease resistance can provide information on the manner in  
31 which complex phenotypes are interrelated. However, studies on statistical methods tailored  
32 to multi-dimensional phenotypes are limited, whereas numerous methods are available for  
33 evaluating the massive number of genetic markers. Factor analysis operates at the level of la-  
34 tent variables predicted to generate observed responses. The objectives of this study were to  
35 illustrate the manner in which data-driven exploratory factor analysis can map observed phe-  
36 notypes into a smaller number of latent variables and infer a genomic latent factor network  
37 using 45 agro-morphological, disease, and grain mineral phenotypes measured in synthetic  
38 hexaploid wheat lines (*Triticum Aestivum L.*). In total, eight latent factors including grain  
39 yield, architecture, flag leaf-related traits, grain minerals, yellow rust, two types of stem rust,  
40 and leaf rust were identified as common sources of the observed phenotypes. The genetic  
41 component of the factor scores for each latent variable was fed into a Bayesian network to  
42 obtain a trait structure reflecting the genetic interdependency among traits. Three directed  
43 paths were consistently identified by two Bayesian network algorithms. Flag leaf-related  
44 traits influenced leaf rust, and yellow rust and stem rust influenced grain yield. Additional  
45 paths that were identified included flag leaf-related traits to minerals and minerals to archi-  
46 tecture. This study shows that data-driven explanatory factor analysis can reveal smaller  
47 dimensional common latent phenotypes that are likely to give rise to numerous observed  
48 field phenotypes without relying on prior biological knowledge. The inferred genomic latent  
49 factor structure from the Bayesian network provides insights for plant breeding to simulta-  
50 neously improve multiple traits, as an intervention on one trait will affect the values of focal  
51 phenotypes in an interrelated complex trait system.

## 52 Background

53 With the development of high-throughput phenotyping technologies, phenomics has been  
54 generating plant measurements at a greater level of resolution and dimensionality (Araus  
55 and Cairns, 2014; Watanabe et al., 2017). Integrating these diverse and heterogeneous data  
56 to improve the biological understanding of plant systems and interpret the underlying inter-  
57 relationships among phenotypes remains challenging (Morota et al., 2019). One approach  
58 is to model each measurement as a different trait using a multi-trait model (Henderson and  
59 Quaas, 1976). However, in a high-dimensional specification, where the number of traits  
60 measured per genotype can reach hundreds or thousands, this approach leads to dramatic  
61 increases in the computational burden or difficulties in interpreting the results. Recently, Yu  
62 et al. (2019) showed that factor analysis can be used to reduce the dimension of response  
63 variables by assuming latent factors that give rise to observed phenotypes in rice. They  
64 used confirmatory factor analysis (CFA), which requires knowledge of the phenotype-factor  
65 category before data analysis. However, reliable phenotype-factor patterns are not always  
66 known in advance. Alternatively, exploratory factor analysis (EFA) can be used to perform  
67 latent variable analysis by estimating patterns from data when a latent structure cannot be  
68 determined a priori. EFA identifies underlying latent factors to represent observed measure-  
69 ments, which is useful when the exact number and meaning of latent factors are unknown  
70 (Jöreskog, 1967; Hoyle and Duvall, 2004).

71 The first objective of this study was to illustrate the utility of EFA for revealing the  
72 underlying genomic latent structure of agronomic or agro-morphological phenotypes for syn-  
73 thetic hexaploid wheat lines (*T. aestivum* L). Grain yield in wheat is influenced by sev-  
74 eral agro-morphological traits. However, successfully incorporating yield-promoting agro-  
75 morphological traits in breeding programs to improve genetic gains requires detailed knowl-  
76 edge of the interrelationships between and among traits. The second objective was to deter-  
77 mine a trait network structure among the genomic latent factors using a Bayesian network.  
78 This is an essential task because breeding programs often aim to improve multiple corre-

79 lated traits concurrently. Knowledge of directed trait networks accounting for the genetic  
80 interdependency among traits can improve the understanding of the manner in which the  
81 selection of one phenotype may increase or decrease the observation of another phenotype,  
82 providing additional insight beyond associations (Valente et al., 2015). The current study  
83 demonstrates the advantages of the joint application of factor analysis and Bayesian network  
84 as a data-driven approach to discover interrelationships between a set of many correlated  
85 traits in wheat.

## 86 **Materials and Methods**

### 87 **Plant materials**

88 A diversity panel of  $n = 123$  synthetic hexaploid wheat lines, derived from an interspecific  
89 cross between wild accessions of goat grass (*Aegilops tauschii* L.) and diverse accessions  
90 of cultivated durum wheat (*Triticum turgidum* L.), was used in this study. These plant  
91 materials were shared by the International Winter Wheat Improvement Program in Turkey  
92 and are available at <http://www.iwwip.org>. Pedigree information and other details on these  
93 lines were reported previously (Bhatta et al., 2018a,c,d). Briefly, the lines originated from  
94 two breeding programs. The first group of synthetics comprises 14 lines developed by Kyoto  
95 University, Japan, from 1 Langdon durum parent crossed with 14 different accessions of *Ae.*  
96 *tauschii*. The second group consists of 109 lines developed by the International Maize and  
97 Wheat Improvement Center from crosses between 6 winter durum wheats and 11 different  
98 *Ae. tauschii* accessions. The synthetic lines used in this study are unique; they were recently  
99 developed (F8–F9 generations) and tested for multiple traits for use in a breeding program.

### 100 **Phenotypic and genotypic data**

101 We analyzed 16 agronomic-, 16 grain mineral-, and 13 wheat rust-related phenotypes in the  
102 current study. Agronomic traits including grain yield (GY), harvest index (HI), biomass  
103 weight (BMWT), grain volume weight (GVWT), flag leaf length (FLL), flag leaf width  
104 (FLW), flag leaf area (FLA), rachis break (RB), sterile spikelet (SP), spike length (SL),  
105 seeds per spike (SPS), spikelet number (SN), fertile spikelet (FS), spike weight (SW), grain  
106 weight per spike (GPS), and spike harvest index (SHI) were measured using previously  
107 described standard procedures (Bhatta et al., 2018a; Morgounov et al., 2018; Hussain et al.,  
108 2017). Grain minerals including arsenic (As), calcium (Ca), cadmium (Cd), cobalt (Co),  
109 copper (Cu), iron (Fe), potassium (K), lithium (Li), magnesium (Mg), manganese (Mn),  
110 molybdenum (Mo), nickel (Ni), phosphorous (P), sulfur (S), titanium (Ti), and zinc (Zn)

111 were measured via inductively-coupled plasma mass spectrometry (ICP-MS, Agilent 7500cx,  
112 Agilent Technologies, Santa Clara, CA, USA) at the University of Nebraska Redox Biology  
113 Center, Proteomics and Metabolomics Core (Guttieri et al., 2015; Bhatta et al., 2018a).  
114 The wheat rust (leaf stem and yellow rusts) disease severity, coefficient of infection, and  
115 infection type were tested under field conditions as previously described (Peterson et al.,  
116 1948; Morgounov et al., 2018; Bhatta et al., 2018d). Wheat rust traits collected from several  
117 locations in Turkey and one location in Kenya included the leaf rust coefficient of infection  
118 (LRCI), leaf rust infection type (LRIT), leaf rust severity (LRS), stem rust coefficient of  
119 infection at Haymana (SRCIH), stem rust infection type at Haymana (SRITH), stem rust  
120 severity at Haymana (SRSH), stem rust coefficient of infection at Kastamonu (SRCIK), stem  
121 rust infection type at Kastamonu (SRITK), stem rust severity at Kastamonu (SRSK), yellow  
122 rust coefficient of infection at Haymana (YRCIH), yellow rust infection type at Haymana  
123 (YRIH), yellow rust severity at Haymana (YRSH), and yellow rust severity at Kastamonu  
124 (YRSK). All lines were genotyped with the genotyping by sequencing technology (Bhatta  
125 et al., 2018c). After setting a minor allele frequency threshold of 0.05, 35,648 markers  
126 remained for analysis.

## 127 **Experimental design and analysis**

The experiments were conducted across several locations in Turkey and one location in Kenya in 2017. The experimental design was an alpha lattice design with two replications (Barreto et al., 1996). A linear mixed model coupled with restricted maximum likelihood implemented in the PROC MIXED procedure in SAS 9.4 (SAS Institute, Inc., Cary, NC, USA) was used to obtain the adjusted means for each trait from the following model (Bhatta et al., 2018b).

$$y_{ijkl} = \mu + r_i + b(r)_{ji} + c_k + gl(ji) + \epsilon_{ijkl},$$

128 where  $y_{ijk}$  is the trait of interest;  $\mu$  is the overall mean;  $r_i$  is the effect of  $i$ th replication;  
129  $b(r)_{ji}$  is the effect of the  $j$ th block within the  $i$ th replication;  $c_k$  is the  $k$ th check;  $g_{lji}$  (new  
130 variable, where check is coded as 0 and entry is coded as 1, and the genotype is considered  
131 a new variable  $\times$  entry) is the effect of the  $l$ th genotype within the  $j$ th incomplete block of  
132 the  $i$ th replication; and  $\epsilon_{ijkl}$  is the residual.

### 133 Exploratory factor analysis

134 Exploratory factor analysis can reveal the latent structure among phenotypes when no hy-  
135 potheses about the nature of the underlying factor can be assumed *a priori*. This section  
136 closely follows the work of Yu et al. (2020). The aforementioned  $t = 45$  phenotypes were  
137 analyzed using EFA by fitting

$$\mathbf{Y} = \mathbf{\Lambda}\mathbf{F} + \mathbf{U}, \quad (1)$$

138 where  $\mathbf{Y}$  is the  $t \times n$  phenotypic matrix;  $\mathbf{\Lambda}$  is the  $t \times q$  matrix of factor loading indicating  
139 the relation between phenotypes and latent common factors;  $\mathbf{F}$  is the  $q \times n$  matrix of latent  
140 factor scores; and  $\mathbf{U}$  is the  $t \times n$  vector of unique effects that is not explained by  $q$  underlying  
141 common factors. The variance-covariance matrix of  $\mathbf{Y}$  is

$$\mathbf{\Sigma} = \mathbf{\Lambda}\mathbf{\Phi}\mathbf{\Lambda}' + \mathbf{\Psi}, \quad (2)$$

142 where  $\mathbf{\Sigma}$  is the  $t \times t$  variance-covariance matrix of phenotypes,  $\mathbf{\Phi}$  is the variance of factor  
143 scores, and  $\mathbf{\Psi}$  is a  $t \times t$  diagonal matrix of unique variance. The elements of  $\mathbf{\Lambda}$ ,  $\mathbf{\Phi}$ , and  $\mathbf{\Psi}$   
144 are parameters of the model to be estimated from the data. We assumed  $\mathbf{\Phi} = \mathbf{I}$  yielding  
145 factors each with unit variance (Jöreskog, 1967; Anderson, 2003). With the assumption  
146 of  $\mathbf{F} \sim \mathcal{N}(\mathbf{0}, \mathbf{I})$ , parameters  $\mathbf{\Lambda}$  and  $\mathbf{\Psi}$  were estimated by maximizing the log-likelihood of  
147  $\mathcal{L}(\mathbf{\Lambda}, \mathbf{\Psi} | \mathbf{Y})$  using the R package psych (Revelle, 2018) along with a varimax rotation (Kaiser,  
148 1958). A threshold of  $\lambda > |0.3|$  was first applied to screen out factor loading values. Then  
149 each phenotype was assigned to only one of the factors based on its largest loading.

150 Parallel analysis was performed to estimate the optimum number of factors from data  
151 in EFA (Horn, 1965; Hayton et al., 2004). This is conducted by generating simulated data  
152 from the observed data. Next, the eigenvalues were extracted until the observed data had  
153 a smaller eigenvalue than the simulated data. The number of eigenvalues was used as the  
154 number of optimum factors.

155 The factor ability of the data set was also assessed by estimating the Kaiser-Meyer-  
156 Olkin measure of sampling adequacy (Cerny and Kaiser, 1977). This criterion measures  
157 the adequacy of the dataset for factor analysis by investigating the correlation and partial  
158 correlation matrices of the phenotypes. The measure of sampling adequacy ranges between  
159 0 to 1, and values closer to 1 are preferred. When the measure of sampling adequacy is less  
160 than 0.5, the dataset is not recommended for factor analysis (Cerny and Kaiser, 1977).

## 161 **Confirmatory factor analysis**

162 Once the phenotype-factor pattern was established by EFA, Bayesian CFA was used to obtain  
163 factor scores. Although EFA and CFA are similar, there are also clear differences. In general,  
164 EFA is used to find a latent structure in data, whereas CFA requires the phenotype-latent  
165 variable category to be known before analysis and is often used to estimate factor scores based  
166 on the structure from EFA. The differences between EFA and CFA are shown in Figure 1. In a  
167 Bayesian setting, all unknowns in equations (1) and (2) were assigned priors. The assignment  
168 of priors was performed according to Yu et al. (2019, 2020) using the default priors in the  
169 blavaan R package (Merkle and Rosseel, 2018). A Gaussian distribution with a mean of zero  
170 and variance of 100 was assigned to the factor loading term. The variance-covariance matrix  
171 of the latent factors followed an inverse Wishart distribution with a scale matrix of an  $8 \times 8$   
172 identity matrix and degree of freedom of 8. Each error variance followed an inverse Gamma  
173 distribution with a shape parameter of 1 and scale parameter of 0.5. The factor scores  
174 of latent variables ( $\mathbf{F}$ ) were sampled from the conditional distribution of  $p(\mathbf{F}|\mathbf{\Lambda}, \mathbf{\Phi}, \mathbf{\Psi}, \mathbf{Y})$   
175 (Lee and Song, 2012) using a data augmentation technique (Tanner and Wong, 1987). The

176 posterior mean of  $\mathbf{F}$  was considered a new phenotype in subsequent analysis. Convergence  
177 was diagnosed by the potential scale reduction factor (PSRF) (Gelman et al., 1992; Brown,  
178 2014). This criterion utilizes at least two Markov chains, which are considered to be mixed  
179 to a stationary status if the ratio of between the chain variance to within the chain variance  
180 is close to 1. In total, two chains, each consisting of 5,000 Markov chain Monte Carlo samples  
181 after 2,000 burn-in samples, were collected to derive the posterior means.

## 182 **Multi-trait genomic best linear unbiased prediction**

A Bayesian multi-trait genomic best linear unbiased prediction model was applied to parti-  
tion inferred latent variables into genetic and environmental components.

$$\mathbf{F} = \mathbf{X}\mathbf{b} + \mathbf{Z}\mathbf{g} + \mathbf{e},$$

183 where  $\mathbf{F}$  is the vector of estimated factor scores,  $\mathbf{X}$  is the incidence matrix of covariates  
184 including the intercept and the top three principal components accounting for population  
185 structure,  $\mathbf{b}$  is the vector of covariate effects,  $\mathbf{Z}$  is the incidence matrix relating the factor  
186 scores of each latent variable to additive genetic effect,  $\mathbf{g}$  is a vector of additive genetic  
187 effect, and  $\mathbf{e}$  is the vector of residuals. Under the infinitesimal model of inheritance,  $\mathbf{g}$   
188 and  $\mathbf{e}$  were assumed to follow a multivariate Gaussian distribution of  $\mathbf{g} \sim N(0, \Sigma_g \otimes \mathbf{G})$   
189 and  $\mathbf{e} \sim N(0, \Sigma_e \otimes \mathbf{I})$ , respectively. Here,  $\mathbf{G}$  is a  $n \times n$  genomic relationship matrix,  $\mathbf{I}$   
190 is a  $n \times n$  identity matrix,  $\Sigma_g$  and  $\Sigma_e$  are variance-covariance matrices of additive genetic  
191 effect and residuals, respectively, and  $\otimes$  is the Kronecker product. The  $\mathbf{G}$  matrix was  
192 set as  $\mathbf{W}\mathbf{W}'/2\sum_{j=1}^m p_j(1-p_j)$ , where  $\mathbf{W}$  is the centered marker incidence matrix taking  
193 the values of  $0 - 2p_j$  for zero copies of the reference allele,  $1 - 2p_j$  for one copy of the  
194 reference allele,  $2 - 2p_j$  for two copies of the reference allele, and  $p_j$  is the allele frequency  
195 at marker  $j = 1, \dots, m$  (VanRaden, 2008). The prior distribution specifications followed  
196 those of Momen et al. (2019). A flat prior was assigned for  $\mathbf{b}$ . The vectors of additive

197 genetic and residual effects were assigned independent multivariate Gaussian priors with  
198 null mean and inverse Wishart distributions for the covariance matrices  $\Sigma_g$  and  $\Sigma_e$ . A Gibbs  
199 sampler was used to obtain posterior distributions. A burn-in of 10,000 samples followed  
200 by an additional 90,000 samples, thinned by a factor of two, resulted in 45,000 available  
201 samples for posterior mean inferences. The MTM R package was used to fit the model  
202 (<https://github.com/QuantGen/MTM>).

## 203 **Bayesian network structure learning**

204 The posterior means of genetic values of latent variables obtained from the Bayesian multi-  
205 trait genomic best linear unbiased prediction model were used to examine the manner in  
206 which the traits are interrelated using a Bayesian network. A Bayesian network is a graphical  
207 representation of the conditional independence among random variables based on a directed  
208 acyclic graph (Heckerman et al., 1995). For example, if an arrow arises from phenotype A  
209 to phenotype B, phenotype A is considered to impact phenotype B directly conditional on  
210 the remaining phenotypes, whereas the absence of an edge implies conditional independence  
211 given the remaining phenotypes. In this study, the Tabu search (Tabu) and Max-Min Hill-  
212 Climbing (MMHC) algorithms were applied to learn the underlying trait network structure  
213 of latent variables at the genetic level using the bnlearn R package (Scutari and Denis, 2014).  
214 These two algorithms were chosen because they yielded a reasonable result in a recent study  
215 (Yu et al., 2019). The Bayesian information criterion (BIC) score was calculated for the  
216 whole network and for each edge. A higher BIC score leads to greater model fit because  
217 the BIC score is rescaled by -2 in the bnlearn package. Additionally, the strength and  
218 uncertainty of the direction of each edge were estimated probabilistically by bootstrapping  
219 (Scutari and Denis, 2014). Before fitting the Bayesian network structure learning algorithms,  
220 genetic values of latent variables were transformed to be uncorrelated to meet the primary  
221 assumption of a Bayesian network (Töpner et al., 2017; Yu et al., 2019).

## 222 **Data availability**

223 The data are available from the previously published studies. The agronomic, grain minerals,  
224 and rust related phenotypic data are available from Bhatta et al. (2018a,d, 2019) and the  
225 marker data are available from Bhatta et al. (2018d).

## 226 Results

### 227 Assessing factorability and factor selection

228 Figure 2 shows the Pearson's correlation coefficients among all observed variables represented  
229 in a heat map. Moderate to high correlations were observed within the spike-, mineral-, and  
230 rust- related traits. Because the objective of factor analysis is to model the interrelationships  
231 between observed traits with a smaller subset of latent variables, the presence of some block  
232 structures in the heat map suggests that our dataset is suited for factor analysis. This  
233 observation was supported by the overall Kaiser-Meyer-Olkin measure of sampling adequacy,  
234 which was estimated as 0.7, indicating that the factorability of the dataset was sufficient.  
235 Parallel analysis was performed to determine the appropriate number of latent variables.  
236 The first eight eigenvalues extracted from the original data were larger than the first eight  
237 eigenvalues obtained from simulated random data. Thus, eight underlying latent variables  
238 were examined in subsequent analysis.

### 239 Factor loading from EFA

240 Factor analysis was performed to understand the biological meaning of the eight latent  
241 factors by investigating the co-variation among measured observations using EFA. Figure 3  
242 summarizes the degree of the contributions of unobserved factors to the observed phenotypes.  
243 Because EFA allows the cross-loading of phenotypes, an additional step is required so that  
244 each phenotype loads only on one factor. A heat map of the estimated factor loading values  
245 for each phenotype is shown in Figure 3A. The results showed that each variable had some  
246 nonzero loadings on several factors. Figure 3B shows the phenotype-latent variable pattern  
247 after selecting the largest loading for each phenotype and imposing a threshold of  $> |0.30|$ .  
248 This resulted in each phenotype loading on only one factor except for GVWT, RB, SP, and  
249 YRSK, which did not load on to any factors. The results showed that all mineral-related  
250 traits including As, Ca, Cd, Co, Cu, Fe, K, Li, Mg, Mn, Mo, Ni, P, S, Ti, and Zn were loaded

251 on the first factor (F1) ranging from 0.34 to 0.98. Seven agronomic traits including FS, SL,  
252 SN, SPS, SW, GPS, and SHI were placed on the second factor (F2) and biologically all appear  
253 to be related to the plant structure. In this category, the lowest loading was estimated for  
254 the SHI (0.44) and the largest for GPS (0.91). The 12 disease-related phenotypes were  
255 distributed among 4 factors (F3, F4, F5, and F6) with a loading of at least 0.8 in their  
256 categories. FLL, FLW, and FLA traits with 0.84, 0.73, and 0.98 loadings, respectively, were  
257 placed on the seventh factor (F7). Finally, GY, HI, and BM loaded on the eighth factor  
258 (F8).

259 Figure 4 shows the overall inferred latent structure of the data. The biological meanings  
260 attached to the eight factors according to the EFA analysis were GYL: grain yield; ARC:  
261 plant architecture; FL: flag and leaf, MIN: minerals; YRD: yellow rust disease; SRDK:  
262 stem rust disease at Kastamonu; SRDH: stem rust disease at Haymana; and LRD: leaf  
263 rust disease. These estimated latent factors were subsequently evaluated to determine their  
264 genetic interrelationships.

## 265 **Confirmatory factor analysis**

266 Table 1 shows the posterior means and their posterior standard deviations of the standardized  
267 loadings, PSRF, and  $R^2$  statistics from the Bayesian CFA. Convergence was diagnosed from  
268 the PSRF of each observed phenotype. The estimated PSRF values for all phenotypes were  
269 close to 1, suggesting that they converged to a stationary status. The result showed that the  
270 eight latent factors strongly contributed to the observed phenotypes. For the latent factor  
271 GYL, the lowest and highest loading values were obtained for HI and GY, respectively. For  
272 the FL latent factor, all three phenotypes presented a loading of at least 0.77. In ARC, the  
273 factor loading values varied from SHI to FS in ascending order. The MIN latent factor was  
274 associated with the 16 observed phenotypes, which was the largest factor. The lowest and  
275 highest loading values were obtained for Ti and Mg, respectively. The remaining four latent  
276 factors including LRD, SRHD, SRKD, and YRD, which are relevant to diseases, showed

277 that the data fit well with  $>0.8$  loading. The extent of  $R^2$  values mostly agreed with the  
278 estimated loadings with a correlation of 0.99.

## 279 **Bayesian network among genomic latent factors**

280 The Bayesian network was used to investigate the interrelationships among the genetic com-  
281 ponents of latent factors. Because SRDH and SRDK capture the same set of phenotypes  
282 with a high correlation (Figure 3) but were collected at different locations, only SRDH was  
283 used for trait network structure analysis. As shown in Figure 5, Tabu yielded six directed  
284 edges from FL to LRD and MIN, from YRD to LRD and GYL, from MIN to ARC, and from  
285 SRDH to GYL. However, MMHC only produced three directed edges that were a subset of  
286 the Tabu network. Thus, the consensus network has common directed edges from FL and  
287 LRD, from YRD to GYL, and SRDH to GYL. These results suggest that there is stronger  
288 evidence that FL, YRD, and SRDH directly influence LRD, GYL, and GYL, respectively. In  
289 both networks, the bootstrapping results revealed that confidence was always higher regard-  
290 ing the presence or absence of edges compared to the directions of edges. The goodness-of-fit  
291 statistics measured by BIC is shown in Table 2. This table shows how well the paths mirror  
292 the dependence structure of the data. According to the BIC values, Tabu yielded a larger  
293 BIC score than the MMHC algorithms for the entire network (-423.61 vs. -437.39). For each  
294 specific path, removing SRDH  $\rightarrow$  GYL resulted in the largest decrease in the BIC score,  
295 suggesting that this path plays the most important role in the network structure. This was  
296 followed by YRD  $\rightarrow$  GYL and FL  $\rightarrow$  LRD. The top three most influential paths in Tabu  
297 formed the network structure of MMHC.

## 298 Discussion

### 299 Data-driven latent variable analysis

300 With the availability of large volumes of measured observations per individual because of re-  
301 cent advances in phenomics, it is critical to develop a phenotype-centric statistical approach.  
302 Factor analysis is an effective method for handling many response variables in a quantitative  
303 genetic framework (Runcie and Mukherjee, 2013; Peñagaricano et al., 2015; Rocha et al.,  
304 2018; Yu et al., 2019, 2020). The central idea behind factor analysis is to model the observed  
305 phenotypes through unobserved latent factors by maximizing the common variance between  
306 correlated phenotypes. In the current study, latent factors were directly inferred from the  
307 field data of physiological and morphological phenotypes in wheat using EFA followed by  
308 estimating their factor scores by CFA. This allowed the analysis of the lower dimensional  
309 data because the number of latent factors was less than the number of observed phenotypes.  
310 The combination of EFA and CFA enabled the evaluation of the genetics of latent factors  
311 that were predicted to give rise to the observed phenotypes. Our results demonstrate that a  
312 data-driven approach for estimating latent factors using EFA is useful because the observed  
313 traits were uniquely assigned to one of the factors with biological interpretations. This con-  
314 trasts with the results of a recent study by Yu et al. (2019), in which observed phenotypes  
315 were classified into factors based on prior biological knowledge. However, in most scenar-  
316 ios, the phenotype-latent variable pattern may be unknown. In contrast, EFA can be used  
317 to perform latent variable analysis by estimating latent factors from data when the latent  
318 structure cannot be determined *a priori*.

319 The interrelationships among latent variables were investigated at the genomic level us-  
320 ing Tabu and MMHC. Based on the BIC values, Tabu resulted in a better fit than MMHC.  
321 This agrees with the findings of recent studies using Bayesian networks (Töpner et al., 2017;  
322 Scutari et al., 2018; Yu et al., 2019). The trait network structure inferred from MMHC was  
323 a subset of that of MMHC. Additionally, the three directed paths identified from MMHC

324 were the top three most important paths in Tabu according to BIC. This suggests that  
325 the networks structures were consistent between Tabu and MMHC. Thus, the trait network  
326 derived from MMHC can be considered the consensus network that is more reliable. The  
327 network structures from Tabu and MMHC may become aligned by increasing the sample  
328 size. Inferring a trait network from observational data is an emerging topic in quantitative  
329 genetics (Valente et al., 2010). Because breeders are often interested in the impact of ex-  
330 ternal intervention or the selection of one trait over other traits, distinguishing undirected  
331 edges from directed edges is important. The trait network learned in this study can also  
332 be integrated into SEM-GWAS, which is a framework to perform multi-trait genome-wide  
333 association analysis derived from structural equation models (Momen et al., 2018, 2019).  
334 The combination of data-driven EFA and Bayesian network approaches is particularly use-  
335 ful for analyzing image-based high-throughput phenotyping data, where relationships within  
336 image-based phenotypes and between classical phenotypes and image-based phenotypes may  
337 not always be obvious.

## 338 **Biological meaning of the inferred relationships**

339 Previous studies revealed the negative genetic associations of yellow and stem rust traits  
340 with grain yield traits. Wheat rust diseases are foliar fungal diseases whose infection on  
341 the flag leaf close to the grain filling period causes a decline in the photosynthetic ability  
342 of the plant, drastically decreasing the grain filling process and reducing the biomass yield,  
343 thousand kernel weight, and harvest index (He et al., 2019; Bhatta et al., 2018a; Herrera-  
344 Foessel et al., 2006). Thus, the reduction of these important traits results in a reduction in  
345 the final grain yield ( $\text{SRDH} \rightarrow \text{GYL}$  and  $\text{YRD} \rightarrow \text{GYL}$ ). Wheat leaf rust may be affected  
346 by flag leaf traits such as FLL, FLW, and FLA ( $\text{FL} \rightarrow \text{LRD}$ ). As the flag leaf area increases,  
347 the surface also becomes greater, increasing the risk of disease infection on the wider and  
348 longer leaves.

349 Flag leaf traits play important roles in the synthesis, translocation, and remobilization

350 of photo-assimilates and minerals to the grains (Sperotto et al., 2013). A recent study on  
351 *Triticum sps.* showed that the flag leaf contains two- to three-fold higher concentrations  
352 of Fe and Zn than the grain mineral concentrations (Hu et al., 2017). They also found  
353 strong positive correlations between leaf and grain Fe and Zn concentrations. Another study  
354 used more than 120 hexaploid wheat lines and reported a significant positive correlation of  
355 flag leaf N concentrations at anthesis with grain Fe, Mn, and Cu (SHI et al., 2013). These  
356 results suggest that flag leaf traits play an important role in determining the grain mineral  
357 concentration, which agrees with our results indicating a direct link from FL to MN.

358 Foliar diseases such as yellow rust, caused by *Puccinia striiformis f. sp. tritici* (*Pst*), is an  
359 important foliar fungal disease of wheat that causes major yield loss (Bhatta et al., 2019).  
360 This disease produces rust pustules on leaves and reduces the process of photosynthesis  
361 and translocation of photosynthate to grain yield traits, which in turn inhibit grain filling,  
362 possibly resulting in a significant reduction in grain weight and ultimately reducing grain  
363 yield (Ye et al., 2019; Murray and Murray, 2005). A recent study on winter wheat germplasm  
364 showed that yellow rust infection seriously damaged the photosynthetic function of leaves at  
365 an earlier stage of grain filling, leading to biomass loss (He et al., 2019). Additionally, the  
366 presence of foliar diseases in wheat is associated with a reduction in the biomass weight and  
367 harvest index by reducing the healthy leaf area and affecting healthy spike growth (Gooding  
368 et al., 2000; Dimmock and Gooding, 2002), indicating that yellow rust traits affected grain  
369 yield-related traits (YRD  $\rightarrow$  GYL).

370 Several studies have reported negative associations between grain minerals and architecture-  
371 related traits. A larger number of seeds per spike and kernel size in wheat is associated with  
372 lower grain mineral accumulation in the grain, which is mainly attributed to the grain mineral  
373 dilution effect (Bhatta et al., 2018a; Guttieri et al., 2015). Similarly, the nitrogen concentra-  
374 tion in the grains depends on their position within the spike Calderini and Ortiz-Monasterio  
375 (2003); Herzog and Stamp (1983), suggesting that spike architecture traits have important  
376 impacts on grain mineral traits (MIN  $\rightarrow$  ARC).

## 377 **Conclusions**

378 This study demonstrates that data-driven latent variable analysis can reveal the underlying  
379 structure of phenotypes on a smaller dimensional scale. Thus, determining the genetic effects  
380 of correlated traits by factor analysis is an efficient approach for learning the minimum  
381 set of core factors contributing to high-dimensional observed phenotypes. Additionally, by  
382 reconstructing a more general structure of genomic latent factors from observed phenotypes  
383 using a Bayesian network, a clearer picture of trait interdependency can be obtained, which  
384 is useful for developing breeding and management strategies for crops such as wheat.

## 385 **Competing interests**

386 The authors declare that they have no competing interests.

## 387 **Funding**

388 This work was supported in part by Virginia Polytechnic Institute and State University  
389 startup funds to GM.

## 390 **Author contribution statement**

391 MM, MB, WH, and GM conceived the study. MM and HY analyzed the data. MM drafted  
392 the manuscript. WH, MB, HY, and GM revised the manuscript. GM supervised and directed  
393 the study. All authors read and approved the manuscript.

## 394 References

- 395 Anderson, T. (2003). An introduction to multivariate statistical analysis (wiley series in  
396 probability and statistics). *July 11*.
- 397 Araus, J. L. and Cairns, J. E. (2014). Field high-throughput phenotyping: the new crop  
398 breeding frontier. *Trends in Plant Science*, 19(1):52–61.
- 399 Barreto, H., Edmeades, G., Chapman, S., and Crossa, J. (1996). The alpha lattice design  
400 in plant breeding and agronomy: generation and analysis. *Drought-and Low N-Tolerant*  
401 *Maize*, page 544.
- 402 Bhatta, M., Baenziger, P., Waters, B., Poudel, R., Belamkar, V., Poland, J., and Morgounov,  
403 A. (2018a). Genome-wide association study reveals novel genomic regions associated with  
404 10 grain minerals in synthetic hexaploid wheat. *International Journal of Molecular Sci-*  
405 *ences*, 19(10):3237.
- 406 Bhatta, M., Morgounov, A., Belamkar, V., and Baenziger, P. S. (2018b). Genome-wide  
407 association study reveals novel genomic regions for grain yield and yield-related traits in  
408 drought-stressed synthetic hexaploid wheat. *International journal of molecular sciences*,  
409 19(10):3011.
- 410 Bhatta, M., Morgounov, A., Belamkar, V., Poland, J., and Baenziger, P. S. (2018c). Un-  
411 locking the novel genetic diversity and population structure of synthetic hexaploid wheat.  
412 *BMC Genomics*, 19(1):591.
- 413 Bhatta, M., Morgounov, A., Belamkar, V., Wegulo, S. N., Dababat, A. A., Erginbas-Orakci,  
414 G., Bouhssini, M. E., Gautam, P., Poland, J., Akci, N., et al. (2019). Genome-wide associ-  
415 ation study for multiple biotic stress resistance in synthetic hexaploid wheat. *International*  
416 *Journal of Molecular Sciences*, 20(15):3667.

- 417 Bhatta, M., Morgounov, A., Belamkar, V., Yorgancilar, A., and Baenziger, P. S. (2018d).  
418 Genome-wide association study reveals favorable alleles associated with common bunt  
419 resistance in synthetic hexaploid wheat. *Euphytica*, 214(11):200.
- 420 Brown, T. A. (2014). *Confirmatory factor analysis for applied research*. Guilford Publica-  
421 tions.
- 422 Calderini, D. F. and Ortiz-Monasterio, I. (2003). Grain position affects grain macronutrient  
423 and micronutrient concentrations in wheat. *Crop Science*, 43(1):141–151.
- 424 Cerny, B. A. and Kaiser, H. F. (1977). A study of a measure of sampling adequacy for  
425 factor-analytic correlation matrices. *Multivariate Behavioral Research*, 12(1):43–47.
- 426 Dimmock, J. and Gooding, M. (2002). The effects of fungicides on rate and duration of grain  
427 filling in winter wheat in relation to maintenance of flag leaf green area. *The Journal of*  
428 *Agricultural Science*, 138(1):1–16.
- 429 Gelman, A., Rubin, D. B., et al. (1992). Inference from iterative simulation using multiple  
430 sequences. *Statistical Science*, 7(4):457–472.
- 431 Gooding, M., Dimmock, J., France, J., and Jones, S. (2000). Green leaf area decline of wheat  
432 flag leaves: the influence of fungicides and relationships with mean grain weight and grain  
433 yield. *Annals of applied Biology*, 136(1):77–84.
- 434 Guttieri, M. J., Baenziger, P. S., Frels, K., Carver, B., Arnall, B., and Waters, B. M. (2015).  
435 Variation for grain mineral concentration in a diversity panel of current and historical  
436 great plains hard winter wheat germplasm. *Crop Science*, 55(3):1035–1052.
- 437 Hayton, J. C., Allen, D. G., and Scarpello, V. (2004). Factor retention decisions in ex-  
438 ploratory factor analysis: A tutorial on parallel analysis. *Organizational Research Methods*,  
439 7(2):191–205.

- 440 He, C., Zhang, Y., Zhou, W., Guo, Q., Bai, B., Shen, S., and Huang, G. (2019). Study on  
441 stripe rust (*Puccinia striiformis*) effect on grain filling and seed morphology building of  
442 special winter wheat germplasm huixianhong. *PLoS ONE*, 14(5):e0215066.
- 443 Heckerman, D., Geiger, D., and Chickering, D. M. (1995). Learning bayesian networks: The  
444 combination of knowledge and statistical data. *Machine Learning*, 20(3):197–243.
- 445 Henderson, C. and Quaas, R. (1976). Multiple trait evaluation using relatives' records.  
446 *Journal of Animal Science*, 43(6):1188–1197.
- 447 Herrera-Foessel, S., Singh, R., Huerta-Espino, J., Crossa, J., Yuen, J., and Djurle, A. (2006).  
448 Effect of leaf rust on grain yield and yield traits of durum wheats with race-specific and  
449 slow-rusting resistance to leaf rust. *Plant Disease*, 90(8):1065–1072.
- 450 Herzog, H. and Stamp, P. (1983). Dry matter and nitrogen accumulation in grains at different  
451 ear positions in gigas, semidwarf and normal spring wheats. *Euphytica*, 32(2):511–520.
- 452 Horn, J. L. (1965). A rationale and test for the number of factors in factor analysis. *Psy-*  
453 *chometrika*, 30(2):179–185.
- 454 Hoyle, R. H. and Duvall, J. L. (2004). Determining the number of factors in exploratory and  
455 confirmatory factor analysis. *Handbook of quantitative methodology for the social sciences*,  
456 pages 301–315.
- 457 Hu, X., Liu, J., Zhang, L., Wu, B., Hu, J., Liu, D., and Zheng, Y. (2017). Zn and fe  
458 concentration variations of grain and flag leaf and the relationship with nam-g1 gene in  
459 triticum timopheevii (zhuk.) zhuk. ssp. timopheevii. *Cereal Research Communications*,  
460 45(3):421–431.
- 461 Hussain, W., Baenziger, P. S., Belamkar, V., Guttieri, M. J., Venegas, J. P., Easterly, A.,  
462 Sallam, A., and Poland, J. (2017). Genotyping-by-sequencing derived high-density linkage

- 463 map and its application to qtl mapping of flag leaf traits in bread wheat. *Scientific Reports*,  
464 7(1):16394.
- 465 Jöreskog, K. G. (1967). Some contributions to maximum likelihood factor analysis. *Psy-*  
466 *chometrika*, 32(4):443–482.
- 467 Kaiser, H. F. (1958). The varimax criterion for analytic rotation in factor analysis. *Psy-*  
468 *chometrika*, 23(3):187–200.
- 469 Lee, S.-Y. and Song, X.-Y. (2012). *Basic and advanced Bayesian structural equation mod-*  
470 *eling: With applications in the medical and behavioral sciences*. John Wiley & Sons,  
471 Hoboken, New Jersey.
- 472 Merkle, E. C. and Rosseel, Y. (2018). blavaan: Bayesian structural equation models via  
473 parameter expansion. *Journal of Statistical Software*, 85(4):1–30.
- 474 Momen, M., Ayatollahi Mehrgardi, A., Amiri Roudbar, M., Kranis, A., Mercuri Pinto, R.,  
475 Valente, B. D., Morota, G., Rosa, G. J., and Gianola, D. (2018). Including phenotypic  
476 causal networks in genome-wide association studies using mixed effects structural equation  
477 models. *Frontiers in genetics*, 9:455.
- 478 Momen, M., Campbell, M. T., Walia, H., and Morota, G. (2019). Utilizing trait networks  
479 and structural equation models as tools to interpret multi-trait genome-wide association  
480 studies. *Plant methods*, 15(1):107.
- 481 Morgounov, A., Abugalieva, A., Akan, K., Akın, B., Baenziger, S., Bhatta, M., Dababat,  
482 A. A., Demir, L., Dutbayev, Y., El Bouhssini, M., et al. (2018). High-yielding winter syn-  
483 thetic hexaploid wheats resistant to multiple diseases and pests. *Plant Genetic Resources*,  
484 16(3):273–278.
- 485 Morota, G., Jarquin, D., Campbell, M. T., and Iwata, H. (2019). Statistical methods for

- 486 the quantitative genetic analysis of high-throughput phenotyping data. *arXiv preprint*  
487 *arXiv:1904.12341*.
- 488 Murray, D. G. and Murray, G. M. (2005). *Stripe rust: Understanding the disease in wheat*.  
489 NSW Department of Primary Industries.
- 490 Peñagaricano, F., Valente, B., Steibel, J., Bates, R., Ernst, C., Khatib, H., and Rosa,  
491 G. (2015). Searching for causal networks involving latent variables in complex traits:  
492 Application to growth, carcass, and meat quality traits in pigs. *Journal of Animal Science*,  
493 93(10):4617–4623.
- 494 Peterson, R. F., Campbell, A., and Hannah, A. (1948). A diagrammatic scale for estimating  
495 rust intensity on leaves and stems of cereals. *Canadian Journal of Research*, 26(5):496–500.
- 496 Revelle, W. (2018). *psych: Procedures for Psychological, Psychometric, and Personality*  
497 *Research*. Northwestern University, Evanston, Illinois. R package version 1.8.12.
- 498 Rocha, J. R. d. A. S. d. C., Machado, J. C., and Carneiro, P. C. S. (2018). Multitrait index  
499 based on factor analysis and ideotype-design: proposal and application on elephant grass  
500 breeding for bioenergy. *GCB Bioenergy*, 10(1):52–60.
- 501 Runcie, D. E. and Mukherjee, S. (2013). Dissecting high-dimensional phenotypes with  
502 bayesian sparse factor analysis of genetic covariance matrices. *Genetics*, 194(3):753–767.
- 503 Scutari, M. and Denis, J.-B. (2014). *Bayesian networks: with examples in R*. Chapman and  
504 Hall/CRC.
- 505 Scutari, M., Graafland, C. E., and Gutiérrez, J. M. (2018). Who learns better bayesian  
506 network structures: Constraint-based, score-based or hybrid algorithms? *arXiv preprint*  
507 *arXiv:1805.11908*.

- 508 SHI, R.-l., TONG, Y.-p., JING, R.-l., ZHANG, F.-s., and ZOU, C.-q. (2013). Characteriza-  
509 tion of quantitative trait loci for grain minerals in hexaploid wheat (*triticum aestivum* l.).  
510 *Journal of Integrative Agriculture*, 12(9):1512–1521.
- 511 Sperotto, R., Ricachenevsky, F., de A Waldow, V., Müller, A., Dressler, V., and Fett, J.  
512 (2013). Rice grain fe, mn and zn accumulation: How important are flag leaves and seed  
513 number? *Plant, Soil and Environment*, 59(6):262–266.
- 514 Tanner, M. A. and Wong, W. H. (1987). The calculation of posterior distributions by data  
515 augmentation. *Journal of the American Statistical Association*, 82(398):528–540.
- 516 Töpner, K., Rosa, G. J., Gianola, D., and Schön, C.-C. (2017). Bayesian networks illustrate  
517 genomic and residual trait connections in maize (*zea mays* l.). *G3: Genes, Genomes,*  
518 *Genetics*, 7(8):2779–2789.
- 519 Valente, B. D., Morota, G., Peñagaricano, F., Gianola, D., Weigel, K., and Rosa, G. J.  
520 (2015). The causal meaning of genomic predictors and how it affects construction and  
521 comparison of genome-enabled selection models. *Genetics*, 200(2):483–494.
- 522 Valente, B. D., Rosa, G. J., Gustavo, A., Gianola, D., and Silva, M. A. (2010). Searching for  
523 recursive causal structures in multivariate quantitative genetics mixed models. *Genetics*.
- 524 VanRaden, P. M. (2008). Efficient methods to compute genomic predictions. *Journal of*  
525 *Dairy Science*, 91(11):4414–4423.
- 526 Watanabe, K., Guo, W., Arai, K., Takanashi, H., Kajiya-Kanegae, H., Kobayashi, M., Yano,  
527 K., Tokunaga, T., Fujiwara, T., Tsutsumi, N., et al. (2017). High-throughput phenotyping  
528 of sorghum plant height using an unmanned aerial vehicle and its application to genomic  
529 prediction modeling. *Frontiers in plant science*, 8:421.
- 530 Ye, X., Li, J., Cheng, Y., Yao, F., Long, L., Wang, Y., Wu, Y., Li, J., Wang, J., Jiang, Q.,

531 et al. (2019). Genome-wide association study reveals new loci for yield-related traits in  
532 sichuan wheat germplasm under stripe rust stress. *BMC Genomics*, 20(1):1–17.

533 Yu, H., Campbell, M. T., Zhang, Q., Walia, H., and Morota, G. (2019). Genomic Bayesian  
534 confirmatory factor analysis and bayesian network to characterize a wide spectrum of rice  
535 phenotypes. *G3: Genes, Genomes, Genetics*, 9(6):1975–1986.

536 Yu, H., Morota, G., Celestino, E. F., Dahlen, C. R., Wagner, S. A., Riley, D. G., and Hanna,  
537 L. L. H. (2020). Deciphering cattle temperament measures derived from a four-platform  
538 standing scale using genetic factor analytic modeling. *Frontiers in Genetics*, 11:599.

## 539 Tables

Table 1: Factor loading values from the Bayesian confirmatory factor analysis. PSD: posterior standard deviation, PSRF: potential scale reduction factor, GYL: grain yield, ARC: plant architecture, FL: flag and leaf, MIN: mineral-related traits, YRD: yellow rust, SRDK: stem rust at Kastamonu, SRDH: stem rust at Haymana, LRD: leaf rust, and  $R^2$ : coefficient of determination.

Latent factor	Phenotype	Loading	PSD	PSRF	$R^2$
GYL:	grain yield	0.998	0.071	1.000	0.996
	harvest index	0.571	0.090	1.000	0.327
	biomass weight	0.823	0.081	1.000	0.677
FL:	flag leaf length	0.849	0.080	1.002	0.720
	flag leaf width	0.771	0.082	1.002	0.594
	flag leaf area	0.999	0.071	1.005	0.998
ARC:	fertile spikelet	0.867	0.098	1.006	0.752
	spike length	0.543	0.097	1.001	0.295
	spikelet number	0.776	0.099	1.005	0.602
	seeds per spike	0.796	0.088	1.001	0.633
	spike weight	0.740	0.110	1.003	0.548
	grain weight per spike	0.854	0.108	1.005	0.730
	spike harvest index	0.462	0.107	1.001	0.214
MIN:	arsenic	0.483	0.098	1.001	0.234
	calcium	0.884	0.086	1.005	0.782
	cadmium	0.767	0.091	1.003	0.588
	colbalt	0.468	0.101	1.001	0.219
	copper	0.940	0.083	1.005	0.883
	iron	0.927	0.084	1.005	0.858
	potassium	0.773	0.091	1.003	0.598
	lithium	0.379	0.102	1.000	0.144
	magnesium	0.984	0.078	1.007	0.968
	manganese	0.928	0.084	1.006	0.861
	molybdenum	0.757	0.091	1.002	0.573
	nickel	0.531	0.098	1.001	0.282
	phosphorous	0.974	0.080	1.007	0.949
	sulphur	0.750	0.091	1.002	0.563
titanium	0.365	0.100	1.000	0.133	
zinc	0.817	0.089	1.003	0.667	
LRD:	leaf rust severity	0.996	0.071	1.016	0.992
	leaf rust infection type	0.813	0.081	1.006	0.662
	leaf rust coefficient of infection	0.998	0.071	1.015	0.997
SRDH:	stem rust severity at Haymana	0.955	0.074	1.002	0.912
	stem rust infection type at Haymana	0.872	0.078	1.001	0.760
	stem rust coefficient of infection at Haymana	0.998	0.071	1.003	0.997
SRDK:	stem rust severity at Kastamonu	0.968	0.073	1.012	0.937
	stem rust infection type at Kastamonu	0.912	0.076	1.009	0.832
	stem rust coefficient of infection at Kastamonu	0.991	0.071	1.012	0.982
YRD:	yellow rust coefficient of infection at Haymana	0.999	0.071	1.002	0.999
	yellow rust infection type at Haymana	0.824	0.080	1.001	0.680
	yellow rust severity at Haymana	0.973	0.073	1.002	0.946

Table 2: Bayesian information criterion (BIC) scores for pairs of nodes reporting the change in the score caused by an arc removal relative to the entire network score. Tabu: Tabu Search, MMHC: Max-Min Hill-Climbing, GYL: grain yield traits, FL: flag and leaf traits, MIN: mineral traits, ARC: architecture traits, LRD: leaf rust disease, SRDH: steam rust disease at Haymana, and YRD: yellow rust disease.

Algorithm	from	to	BIC
Tabu	FL	MIN	-2.074
	FL	LRD	-9.648
	MIN	ARC	-5.884
	SRDH	GYL	-32.297
	YRD	GYL	-16.399
	YRD	ARC	-5.916
MMHC	FL	LRD	-5.989
	SRDH	GYL	-32.297
	YRD	GYL	-16.3997

## 540 Figures

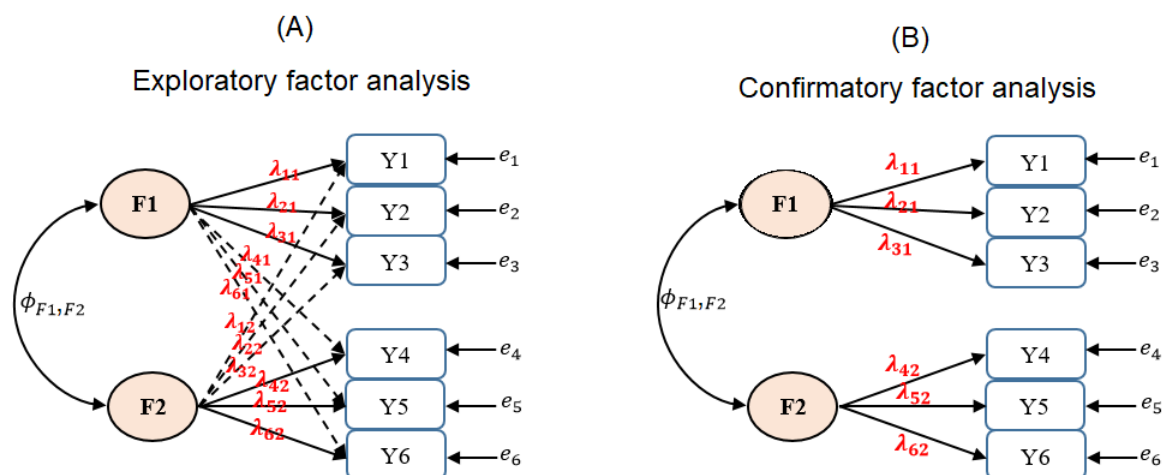


Figure 1: A graphical representation of exploratory factor analysis (panel A) and confirmatory factor analysis (panel B) assuming that there are hypothetical six observed phenotypes ( $Y_1, Y_2, \dots, Y_6$ ) and two unobserved latent factors (F1 and F2). The double headed arrow is the covariance between the two latent factors ( $\Phi_{F1, F2}$ ).  $e_1, e_2, \dots, e_6$  represent the residuals. Exploratory factor analysis estimates the phenotype-factor relationship from the data by allowing cross-loading. By choosing the largest factor loading value for each phenotype, phenotypes can be uniquely assigned to one of the two factors. In this example,  $Y_1, Y_2$ , and  $Y_3$  loaded on the F1 (with loadings of  $\lambda_{11}, \lambda_{21}$ , and  $\lambda_{31}$ ) and  $Y_4, Y_5$ , and  $Y_6$  loaded on F2 (with loadings of  $\lambda_{42}, \lambda_{52}$ , and  $\lambda_{62}$ ). Confirmatory factor analysis assumes that this relationship is known *a priori*.

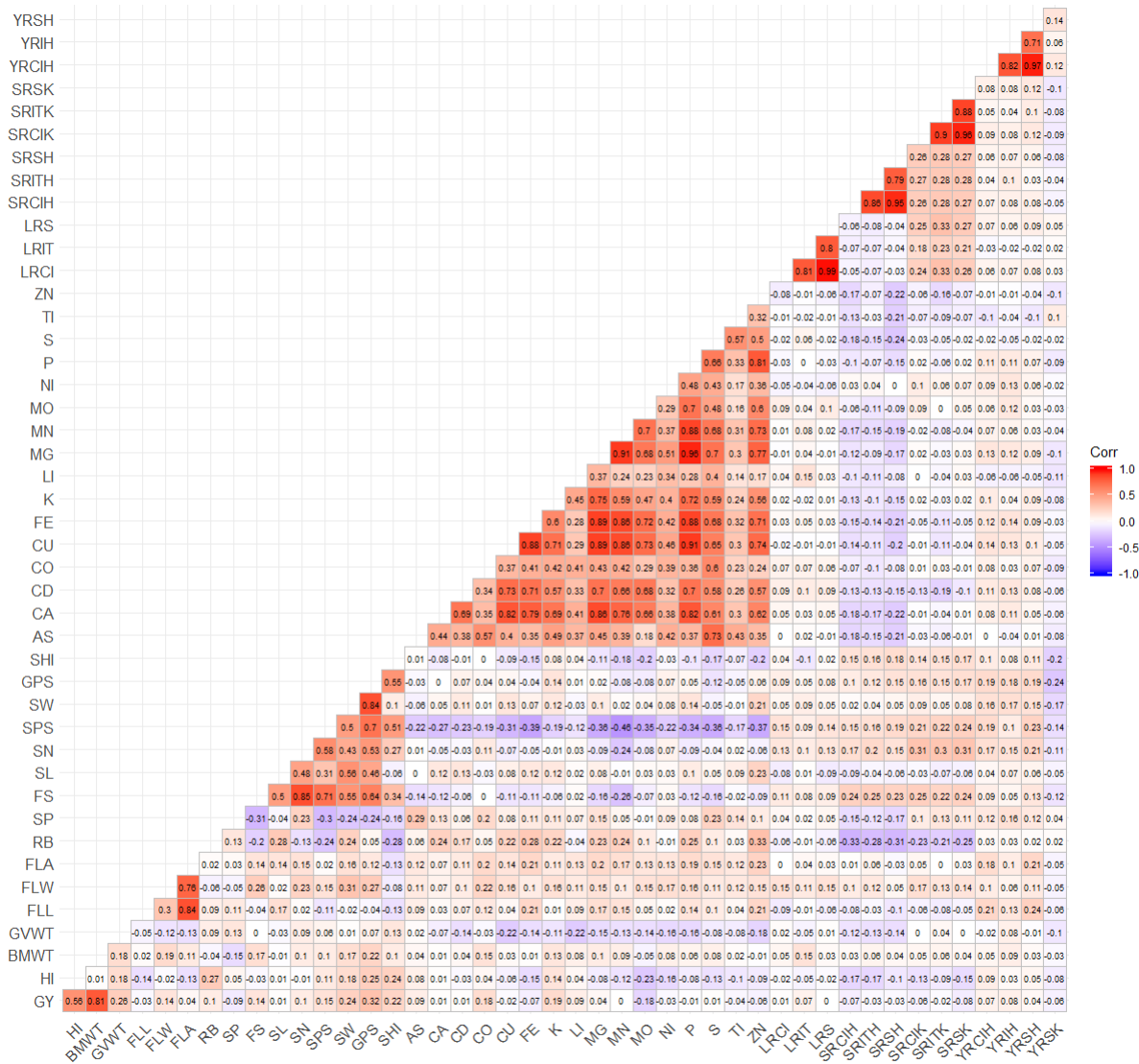


Figure 2: Pairwise Pearson's correlations between 45 phenotypes. GY: grain yield, HI: harvest index, BWT: biomass weight, GVWT: grain volume weight, FLL: flag leaf length, FLW: flag leaf width, FLA: flag leaf area, SL: spike length, SN: spikelet number, SP: sterile spikelet, FS: fertile spikelet, RB: rachis break, SPS: seeds per spike, SW: spike weight, GPS: grain weight per spike, SHI: spike harvest index, AS: arsenic, CA: calcium, CD: cadmium, CO: cobalt, CU: copper, FE: iron, K: potassium, LI: lithium, MG: magnesium, MN: manganese, MO: molybdenum, NI: nickel, P: phosphorous, S: sulphur, TI: titanium, ZN: zinc, LRCI: leaf rust coefficient of infection, LRIT: leaf rust infection type, LRS: leaf rust severity, SRCIH: steam rust coefficient of infection at Haymana, SRITH: stem rust infection type at Haymana, SRSH: stem rust severity at Haymana, SRCIK: stem rust coefficient of infection at Kastamonu, SRITK: stem rust infection type at Kastamonu, SRSK: stem rust severity at Kastamanu, YRCIH: yellow rust coefficient of infection at Haymana, YRIH: yellow rust infection type at Haymana, YRSH: yellow rust severity at Haymana, YRSK: yellow rust severity at Kastamonu.



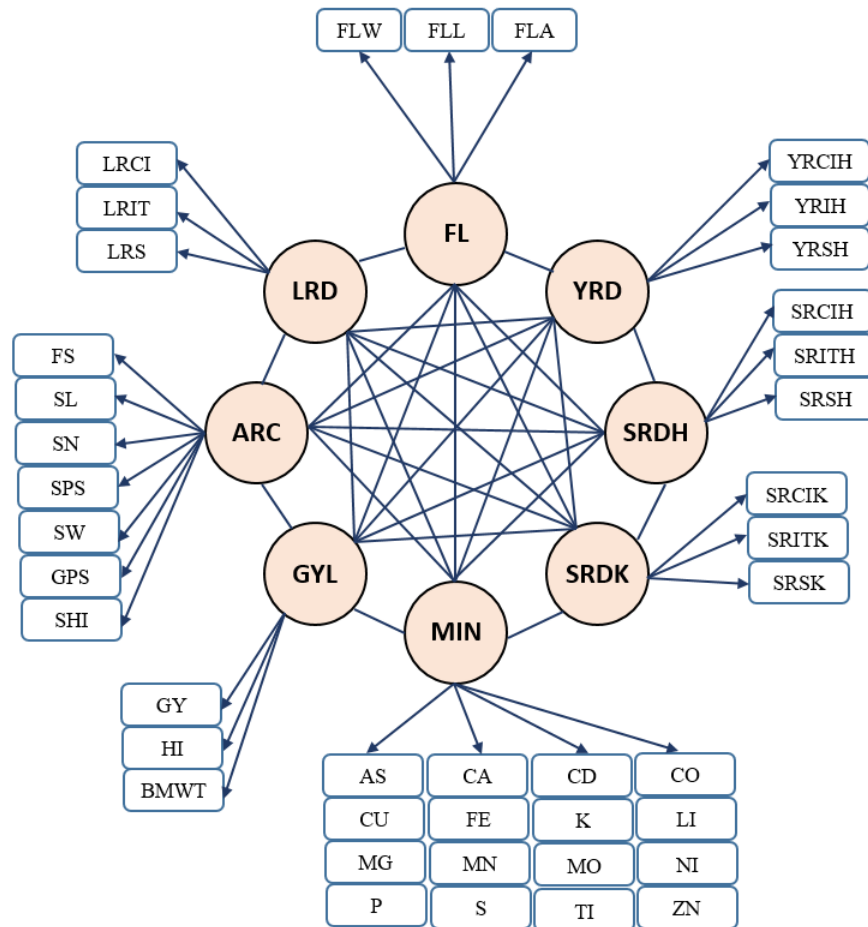


Figure 4: Relationship between eight latent variables and observed phenotypes based on explanatory factor analysis. GYL: grain yield related traits, ARC: architecture related trait, FL: flag and leaf related traits, MIN: mineral-related traits, YRD: yellow rust related traits, SRDK: stem rust related traits at Kastamonu, SRDH: stem rust related traits at Haymana, LRD: leaf rust related traits. The eight latent factors were assumed to be correlated. Abbreviations of observed phenotypes are shown in Figure 2.

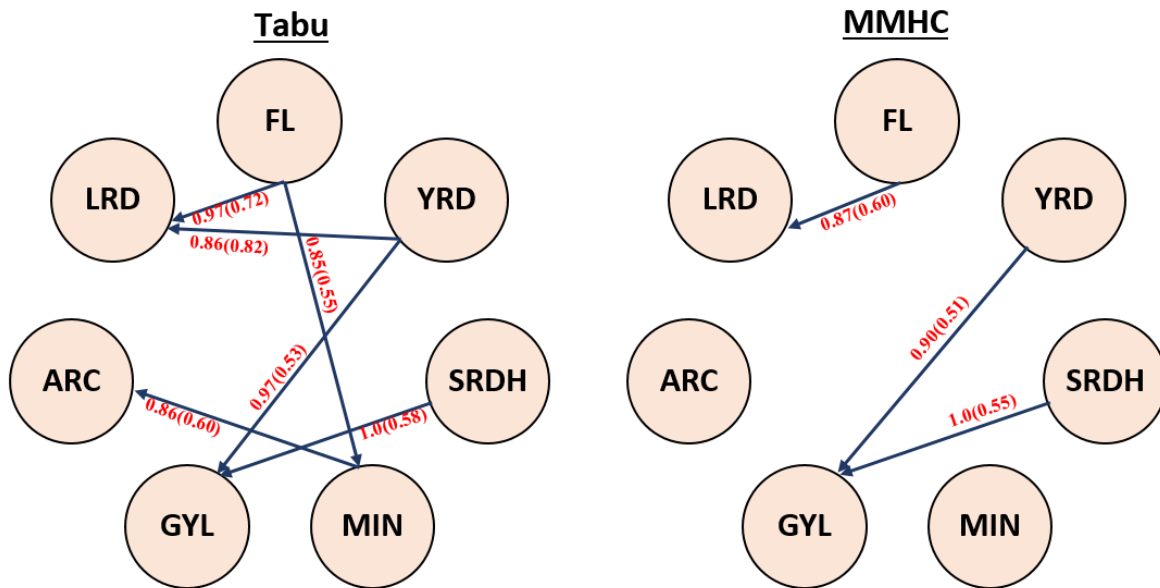


Figure 5: Bayesian networks learned from Tabu search (Tabu) and Max-Min Hill-Climbing (MMHC). Structure learning test was performed with 5,000 bootstrap samples. Labels of the edges refer to the strength and direction (parenthesis) which measure the confidence of the directed edge. The strength indicates the frequency of the edge is present and the direction measures the frequency of the direction conditioned on the presence of edge. GYL: grain yield related traits, ARC: architecture related trait, FL: flag and leaf related traits, MIN: mineral-related traits, YRD: yellow rust related traits, SRDK: stem rust related traits at Kastamonu, SRDH: stem rust related traits at Haymana, LRD: leaf rust related traits.